Int. J. Electrochem. Sci., 12 **(2017)** 1157 – 1166, doi: 10.20964/2017.02.41

International Journal of
ELECTROCHEMICAL
SCIENCE
www.electrochemsci.org

Asymmetric Supercapacitors with High Energy and Power Density Fabricated Using $LiMn_2O_4$ Nano-rods and Activated Carbon Electrodes

Jing Li[1,2*], *Jianqiang Guo*[1,2*], *Xia Zhang*[1,2], *Yeju Huang*[3], *Lei Guo*[1]

[1] School of Materials Science and Engineering, Southwest University of Science and Technology, Mianyang 621010, China
[2] State Key Laboratory Cultivation Base for Nonmetal Composites and Functional Materials, Southwest University of Science and Technology, Mianyang 621010, China
[3] School of National Defence Science and Technology, Southwest University of Science and Technology, Mianyang 621010, China
[*]E-mail: 1035698254@qq.com

Received: 16 November 2016 / *Accepted:* 19 December 2016 / *Published:* 30 December 2016

A novel asymmetric Li ions supercapacitor was fabricated using $LiMn_2O_4$ nano-rods and activated carbon (AC) electrodes as cathode and anode, respectively. The $LiMn_2O_4$ nano-rods that derived from β-MnO_2 nano-rods not only provide more active sites for charge-transfer reaction, but also served as an energy source to supply a high energy density. The test results showed that the highest energy density of Li ions supercapacitor at the rate of 30 C achieved 33.16 Wh/kg, which was closed to 2.04 times than that of AC/AC supercapacitor. Meanwhile, a large power density had been sustained. In addition, because of low cost and toxicity, easy synthesis, and an abundant resource of $LiMn_2O_4$, this novel asymmetric Li ions supercapacitors could be considered as promising energy storage devices for next generation supercapacitors.

Keywords: β-MnO_2 nanorods; $LiMn_2O_4$ nanorods; activated carbon; asymmetric supercapacitor

1. INTRODUCTION

The fast development of global economy is usually accompanied by a tremendous consumption of energy. The traditional energy, such as coal, fossil oil, gas, will be exhausted unavoidably in the near future [1-4]. Therefore, it is urge and important to develop devices for new energy storage and conversion. Supercapacitor is such an important energy storage device that can bridge the power/energy gap between traditional dielectric capacitors and regular batteries/fuel cells [5-8]. It has

received a considerable attention because of the outstanding properties, such as a high power density, a long cycle life and rapid charge–discharge rates [9, 10]. But one drawback of most commercial supercapacitors based on carbon electrodes is a low energy density, which hinders a large-scale application of supercapacitors. Up to now, many efforts had been made aiming at a high energy density without sacrificing a high power capacity [11-16]. Apart from increasing the specific capacitance of electrodes, an attractive approach is to develop asymmetric supercapacitors, which can increase the operating voltage window by using two different electrodes, resulting in a considerable energy density [17-20]. Regarding the combination of the advantages of both battery electrodes and capacitor electrodes, asymmetric supercapacitors will be one of the most promising energy storage and conversion devices [21-23].

In current work, we had designed and fabricated a novel asymmetric Li ions supercapacitors using $LiMn_2O_4$ nano-rods and activated carbon (AC) electrodes as cathode and anode, respectively. As shown in Fig. 1, the Li^+, which is released from $LiMn_2O_4$ cathode, crossed through electrolyte to the AC anode during the charging process. Meanwhile, the electric double layer is formed on the surface of AC anode. In contrast, the Li^+ of adsorption surface activated carbon embeds in the cathode materials forming the $LiMn_2O_4$ at the process of discharge. As a result, the lithium ions embedding produces the capacity. In this system, the $LiMn_2O_4$ nano-rods that derived from β-MnO_2 nano-rods not only provide more active sites for charge-transfer reaction, but also served as an energy source to supply a high energy density. Moreover, the activated carbon electrode with a high specific area provided a guarantee of good cycle and rate performances. By changing the ratio of $LiMn_2O_4$ nano-rods to AC, the asymmetric Li ions supercapacitors with good overall properties had been obtained. In addition, because of low cost and toxicity, easy synthesis, and an abundant resource of $LiMn_2O_4$, this novel asymmetric Li ions supercapacitors could be considered as promising energy storage devices for next generation supercapacitors.

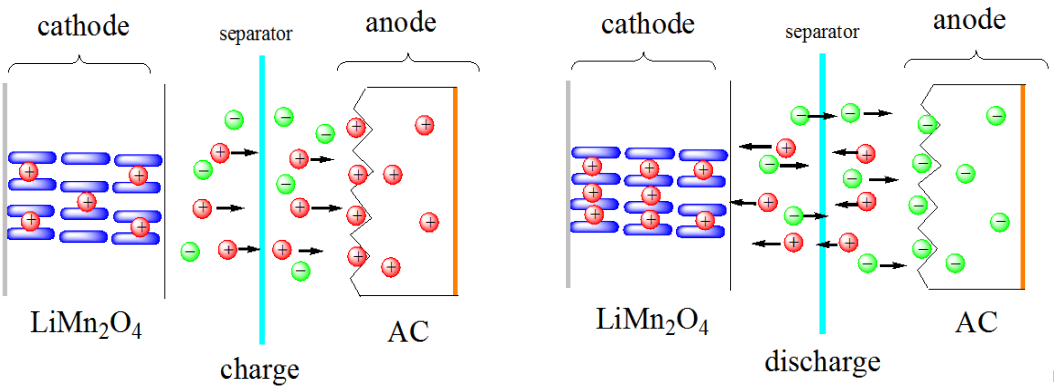

Figure 1. The schematic mechanism of LMO-NRS/AC asymmetric supercapacitor.

2. EXPERIMENTAL

2.1. Material preparation

All the reagents used in our experiments were analytical grade and used without further purification. $LiMn_2O_4$ nanorods were synthesized by using a two-step method. First, the precursor of

β-MnO_2 nanorods were synthesized according the previous report. Typically, 10 mmol $MnSO_4$ and 10 mmol $(NH_4)_2S_2O_8$ were dissolved in 140 ml of distilled water to form a homogeneous solution under magnetically stirring at room temperature. The mixed solution was transferred to a 200 ml Teflon-lined stainless autoclave and heated at 120 °C for 12 h. The resultant precipitate was washed with deionized water and ethanol in succession to remove the sulfate ions and other remnants. The obtained black powder was subsequently dried at 80 °C for 24 h in air to obtain the β-MnO_2 precursor [24]. The next step is the synthesis of single-crystalline $LiMn_2O_4$ nanorods by a solid-state reaction technique using the as-synthesized *β*-MnO_2 nanorods as self-sacrifice precursor. The detailed processes were described as following: a certain amount of β-MnO_2 and $LiOH·H_2O$ (Li/Mn =1.05:2 with the molar ratio) was dispersed into 3 ml anhydrous alcohol to form a thick slurry, which was further ground to form a fine mixture for several hours, and then dried at room temperature. The above process was repeated three times to obtain a well-mixed powder. Subsequently, the samples were calcined in tube furnace under an air atmosphere with temperature controlled from room temperature to 750 °C at a heating rate of 10 °C/min, and cooled naturally to room temperature. The mixture was kept at 500 °C and 750 °C for 4h and 10 h, respectively. Then, nano-rods like $LiMn_2O_4$ products were obtained.

2.2 Materials Characterization

X-ray power diffraction (XRD) spectra of samples were recorded with Cu K*α* radiation (λ= 0.15406 nm) in the diffractometer (X'Pert PRO). The scanning range of diffraction angle (2*θ*) was 3-80°. The morphologies of samples were observed by a field-emission source scanning electron nanoscope (FESEM; Zeiss-Leo Ultra 55).

2.2 Electrochemical measurement

The electrochemical measurements were performed by using CR2016 coin-type cells with active carbon as the negative electrode and $LiMn_2O_4$ nanorods as the positive electrode. The positive electrode was constituted from 75% synthesized product as cathode material, 15% carbon black as conductive agent, and 10% polyvinylidene fluoride (PVDF) as binder dissolved in N-methyl-2-pyrrolidone (NMP). The electrode mixture was pasted on the aluminum foil, and dried at 80 ^oC for 24 h, and then compressed to obtain round positive plates (average diameter 15 mm). According to the same quality ratio the steps with the experiment, using AC (YP-50), conductive carbon black and PVDF binder made negative. In glove box filled with argon gas (MBRAUN, H_2O<0.1 ppm, O_2<0.1 ppm), the Celgard2300 polypropylene nanoporous membrane was used as diaphragm, and the 1 M lithium hexafluorophosphate ($LiPF_6$) in a mixture solvent of the ethylene carbonate (EC), diethyl carbonate (DEC) and dimethyl carbonate (DMC) at a volume ratio of 1:1:1 was used as the electrolyte were assembled the LMO-NRS/AC supercapacitor of (m_+/m_-)= 0.50, 1.00, 1.50 and 2.00. Taking two pieces of quality activated carbon electrode with the same size, the traditional organic AC/AC EDLC were assembled with 1.0 $mol·L^{-1}$ Et_4NBF_4/PC electrolyte and TF4840 capacitance diaphragm, and tested in the voltage range of 0 ~ 2.5 V. The potential change of positive and negative at the same time

for LMO-NRS/AC supercapacitor was detected using three electrodes mould (3ESTC15) with metallic lithium (Beijing, AR) as reference electrode. The potential ranges of LMO-NRS as cathode was limited in 4.4 ~ 3.7 V (vs Li^+/Li). The galvanostatic charge-discharge tests were investigated by a LAND CT2001A battery testing system in the voltage range of 0 ~ 2.3 V. The specific capacity, energy densities and power densities in the full-cell devices were calculated according to the following equations [25]:

$$C_{cell} = \frac{I\Delta t}{M\Delta V} \quad (1)$$

$$E = \frac{1}{2} C_{cell} \Delta V^2 \quad (2)$$

$$P = \frac{E}{\Delta t} \quad (3)$$

where C_{cell} applies to the specific capacitance of a full cell, E is the energy density and P is the power density, I denotes the discharge current, Δt refers to the total discharge time, M represents the total mass of the active materials including both the positive and negative electrodes ($M = m^+ + m^-$) and ΔU is the potential drop during discharge.

3. RESULTS AND DISCUSSION

3.1. Structure and morphology analyses of β-MnO_2 and $LiMn_2O_4$ nanorods

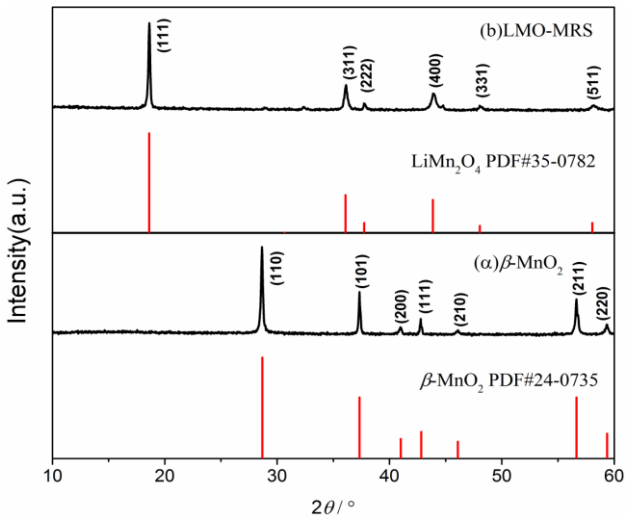

Figure 2. The XRD patterns of the obtained β-MnO_2 and $LiMn_2O_4$ nanorods.

Fig. 2(a) shows the XRD patterns ofβ-MnO_2 that was obtained by one-step hydrothermal method. The characteristic diffraction peaks at 28.68º, 37.33º, 41.01º, 42.82º, 56.65ºand 59.37º can be respectively indexed into (110), (101), (200), (111), (210), (211), (220) planes of β-MnO_2 (JCPDS card No. 24-0735), indicating high purity of the β-MnO_2 products. The sharp and narrow diffraction peaks with no additional impurity phase suggest that the β-MnO_2 has high crystallinity. As

shown in Fig. 2(b), there are six sharp peaks located at 18.61°, 36.09°, 37.75°, 43.86°, 48.05°, and 58.06°, corresponding to (111), (311), (222), (400), (331), (511) planes of $LiMn_2O_4$ (JPCDS 35-0782) [26], respectively. No diffraction peaks of β-MnO_2 can be detected. The results indicate that a relatively high crystallinity of $LiMn_2O_4$ nanorods were successfully synthesized by using the above β-MnO_2 as precursor, and the β-MnO_2 was fully transformed into $LiMn_2O_4$ nanorods.

Fig. 3(a, b) show the SEM images of β-MnO_2. It can be seen that the β-MnO_2 presents the shape of nanorods. The average diameter and length of these nanorods is 300 nm and 1.8 μm, respectively. The rod-like nanostructure of the β-MnO_2 can be further confirmed from the SEM images as shown in Fig. 3(b). Fig. 3(c, d) show the SEM images of the synthesized $LiMn_2O_4$ nanorods via solid-state reaction by using β-MnO_2 nanorods as the precursor. It can be observed that the obtained $LiMn_2O_4$ nanorods have a diameter of about 363 nm and a length of 2.3 μm. The results show that the rod-like morphology of β-MnO_2 nanorods can still maintain after the high temperature solid-state reaction. Compared with β-MnO_2 nanorods, the diameter and length of the $LiMn_2O_4$ nanorods increase, which may be ascribed to crystal lattice transformations during the high temperature solid-state reaction.

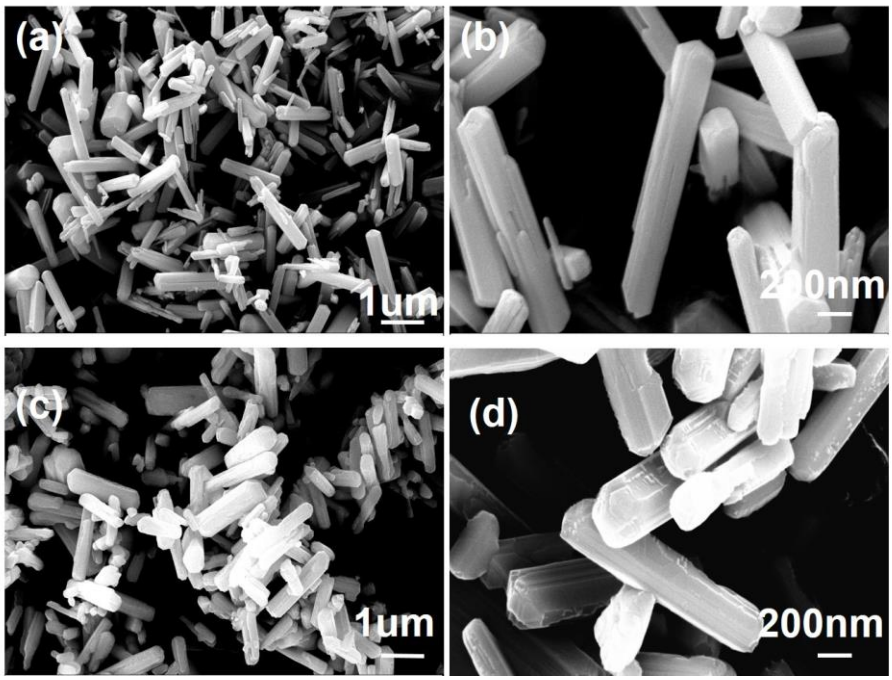

Figure 3. The FESEM images of the obtained (a-b) β-MnO_2 and (c-d) LMO-NRS.

3.2. Electrochemical performance of LMO-NRS/AC asymmetric supercapacitors

In order to monitor the potentials of both cathode and anode electrodes of LMO-NRS/AC asymmetric supercapacitors during the electrochemical cycles, the three-electrode full cells using LMO-NRS cathode and AC anode were assembled, and the weight ratio of active material in cathode to that in anode (m_+/m_-) for the LMO-NRS/AC asymmetric supercapacitors is 0.50, 1.00, 1.50 and

2.00, respectively. The three electrode cells were galvanostatically charged and discharged in the voltage range between 0.0 and 2.3 V at a constant current density of 0.5 C. Fig. 4a-d display the voltage profiles vs. Li^+/Li reference electrode for both cathode and anode electrode. It can be seen that the cathode potential maintained at 4 V platform, only having larger deviation at the end of discharge, while the anode keeps linearly shape. For (m_+/m_-) =0.50, the cathode and anode potentials swing from 3.37 to 4.37 V and from 3.37 to 2.07 V vs. Li^+/Li, respectively. The platform increased to 4.37 V due to the polarization of relative small LMO-NRS content. At the same time, the effective working voltage of supercapacitor is at 2.1 V. For (m_+/m_-) =1.00, 1.50 and 2.00, the polarization of the cathode is not obvious and the working voltage of the supercapacitors is 2.3 V. The cell voltage and the anode potential profiles reveal obvious capacity characteristic due to the capacity contribution of AC. The voltage versus time curves are linearly proportional to the charge-discharge time within the cell voltage window[26]. The cathode potential approaches 4V platform and the negative potential range increases with the increase of LMO-NRS content. However, the capacity of (m_+/m_-) =2.00 is the lowest, the cathode and anode potential ranges decrease to 3.79-3.88 V and 3.76-1.58 V, respectively. Hence, when the LMO-NRS content is relatively large, the change of positive potential is limited.

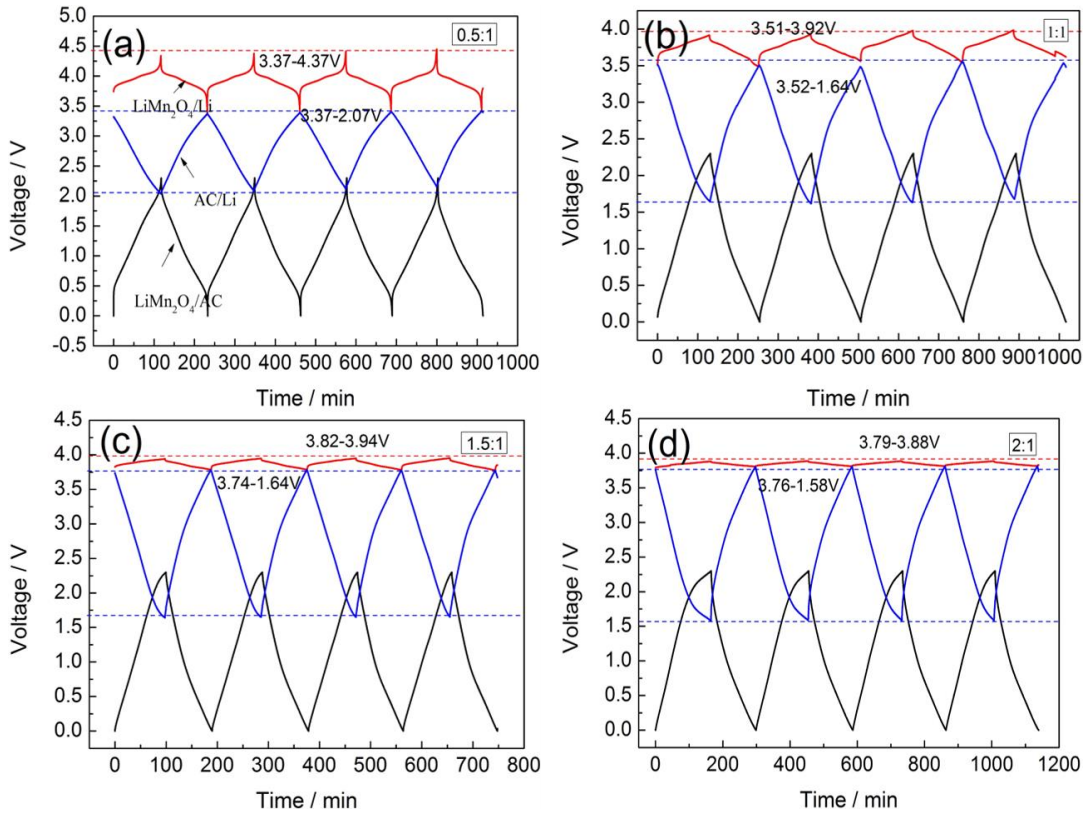

Figure 4. Galvanostatic charge-discharge profiles during the first four cycles for three-electrode LMO-NRS/AC supereapacitors (m_+/m_-) in the voltage range of 0.0-2.3 V at a current density of 0.5 C: (a) 0.5 (b)1.0 (c)1.5 (d)2.0.

The rate capability of AC/AC symmetric supercapacitor and the different weight ratio of LMO-NRS/AC asymmetric supercapacitor was tested by galvanostatic charge-discharge measurement at

different current densities. As shown in Fig. 5, the specific capacity of 0.5 ratio is 3 times higher than AC/AC symmetric supercapacitor at the current density of 2 C. Even when the current density is improved to 30 C, the specific capacity still remain to be 2 times than AC/AC symmetric supercapacitor. Besides, the ratio of 0.5 LMO-NRS/AC asymmetric supercapacitor demonstrates the best rate capability among different ratio of LMO-NRS/AC asymmetric supercapacitors. As it is known to all, when the content of LMO-NRS is relatively high, the capacity contributions of the cell dominate the charge storage in anode electrode. Therefore, the specific capacities of 1.5 and 2 ratio LMO-NRS/AC supercapacitors decrease greatly with the increase of current density.

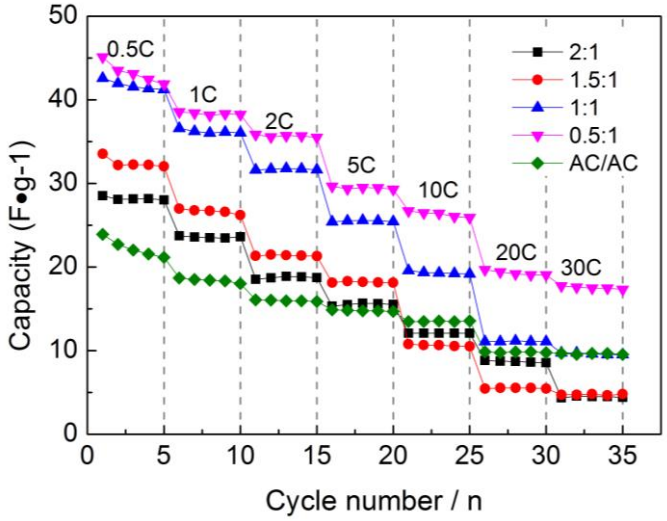

Figure 5. The rate performance of AC/AC and LMO-NRS/AC asymmetric supercapacitor at various current density from 0.5 C to 30 C.

Fig.6 shows the galvanostatic charge-discharge cycling performance of LMO-NRS/AC asymmetric supercapacitors with different weight ratio during the voltage range of 0.0-2.3 V at a current density of 2 C. As shown in Fig.6, the capacity retentions of AC/ AC and LMO-NRS/AC supercapacitor for (m_+/m_-) =0.50 is 100% and 98 % during 1000 cycles, respectively. However, as for the LMO-NRS/AC asymmetric supercapacitors, with the increase of LMO-NRS content, the polarization of LMO-NRS is very obvious. The lattice stability of LMO-NRS is reduced, the electrolyte oxidation occurrs more side effects, which exacerbate the capacity of supercapacitor attenuation. Therefore, considering the stability of the LMO-NRS and application requirements, such as life and apply current range, the optimal weight ratio for LMO-NRS/AC asymmetric supercapacitor is thought to be 0.5, which can make the supercapacitor longer life.

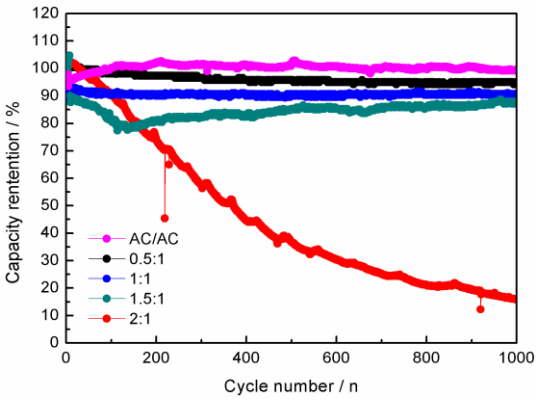

Figure 6. The cycle performance of AC/AC and LMO-NRS/AC supercapacitor at a current density of 2 C.

The energy density and power density for AC/AC symmetric supercapacitor and LMO-NRS/AC asymmetric supercapacitor with different weight ratio are calculated. Fig. 7 shows the energy densities and power densities of AC/AC and LMO-NRS/AC supercapacitors. As shown in Fig. 7, the 0.5 ratio of LMO-NRS/AC asymmetric supercapacitor demonstrates much higher gravimetric energy density than other different ratio of LMO-NRS/AC asymmetric supercapacitors. Besides, the energy densities are 33.16 $Wh \cdot kg^{-1}$ at 16.58 $W \cdot kg^{-1}$, 28.32 $Wh \cdot kg^{-1}$ at 28.32 $W \cdot kg^{-1}$, 26.34 $Wh \cdot kg^{-1}$ at 52.67 $W \cdot kg^{-1}$, 21.78 $Wh \cdot kg^{-1}$ at 108.9 $W \cdot kg^{-1}$, 19.62$Wh \cdot kg^{-1}$ at 196.2 $W \cdot kg^{-1}$, 14.44$Wh \cdot kg^{-1}$ at 288.8$W \cdot kg^{-1}$, 13.02$Wh \cdot kg^{-1}$ at 394.7$W \cdot kg^{-1}$ for 0.5 ratio of LMO-NRS/AC, which is almost 2.04 times than that of traditional AC/AC supercapacitor. However, the energy density decreased with the increase of LMO-MRS content. The reason is that the increase of LMO-MRS content exacerbates the polarization of LMO-MRS electrode. The specific capacities for (m+/m-) =1.50 and 2.00 decrease greatly with the increase of LMO-MRS content. Therfore, the supercapacitors have the relatively low specific energy. On the one hand, because of the LMO-MRS electric polarization is serious, the specific capacitance drops quickly [27, 28].

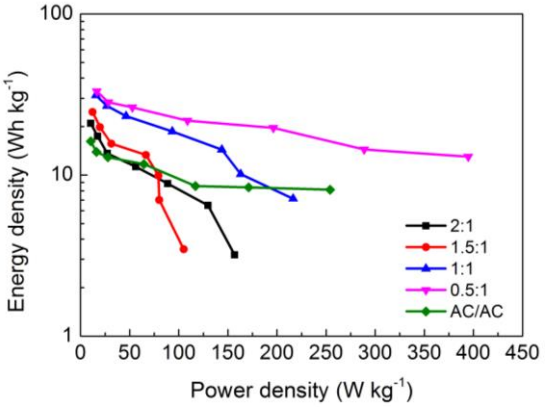

Figure 7. Energy density and power density of AC/AC and LMO-NRS/AC supercapacitors (on the gravimetric basis).

In detail, the comparison of electrochemical performance is listed in Table 1. It can be seen that the LMO-NRS/AC supercapacitors exhibit excellent cycle performance. Besides, the LMO-NRS/AC supercapacitors show higher energy density than other similar Li ions supercapacitors.

Table 1. Comparison of electrochemical performance with other Li ions supercapacitors.

Materials	Current densities ($mA\ g^{-1}$)	capacity retentions (%) (cycle number)	Reference
LMO-NRS/AC	33.16	98 (1000)	This work
$Li_4Ti_5O_{12}$/AC	28.5	98 (1000)	29
$LiNi_{0.5}Co_{0.2}Mn_{0.3}O_2$/ AC	no reference	63 (1000)	30

Based on the above results, it can be found that the LMO-NRS/AC asymmetric supercapacitors present higher electrochemical performance than AC/AC symmetric supercapacitors. Besides, the 0.5 ratio of LMO-NRS/AC asymmetric supercapacitor holds the highest energy density among all supercapacitors. As a result, the optimal weight ratio (m+/m-) for LMO-NRS/AC asymmetric supercapacitors is thought to be 0.5.

4. CONCLUSIONS

In present work, $LiMn_2O_4$ nano-rods were successfully synthesized by using β-MnO_2 as precursor. Moreover, the as-synthesized $LiMn_2O_4$ nano-rods exhibit superior rate performance as cathode in the asymmetric supercapacitor. More importantly, the energy densities of various weight ratio of LMO-NRS/AC asymmetric supercapacitors were studied, suggesting the 0.5 ratio of LMO-NRS/AC asymmetric supercapacitor holds the highest energy density among all supercapacitors.

ACKNOWLEDGMENT
This research was supported by the National Natural Science Foundation of China (Grant No. 14Zg1102) and Postgraduate Innovation Fund Project by Southwest University of Science and Technology (Grant No. 15ycx018).

References

1. M. Armand, F. Endres, D. R. MacFarlane, H. Ohno and B. Scrosati, *Nat. Mater*., 8 (2009) 621.
2. C. Z. Yuan, X. G. Zhang, B. Gao and J. Li, *Mater. Chem. Phys*., 101 (2007) 148.
3. Z. Chen, Y. C. Qin, D. Weng, Q. F. Xiao, Y. T. Peng, X. L. Wang, H. X. Li, F. Wei and Y. F. Lu, *Adv. Funct. Mater*., 19 (2009) 3420.
4. K. W, Nam and K. B. Kim, *J. Electrochem. Soc*., 149 (2002) A346.

5. D. P. Aurelien, I. Plitz, S. Menocal and G. Amatucci, *J. Power Sources*, 115 (2003) 171.
6. P. C. Chen, G. Z. Shen, Y. Shi, H. T. Chen and C. W. Zhou, *ACS Nano*, 4 (2010) 4403.
7. J. Yan, Z. J. Fan, W. Sun, G. Q. Ning, T. Wei, Q. Zhang, R. F. Zhang, L. J. Zhi and F. Wei, *Adv. Funct. Mater.*, 22 (2012) 2632.
8. V. Khomenko, E. Raymundo-Pinero and F. Béguin, *J. Power Sources*, 153 (2006) 183.
9. Y. G. Wang and Y. Y. Xia, *Electrochem. Commun*., 7 (2005) 1138.
10. T. Brousse and D. Bélanger, *Electrochem. Solid State Lett*., 6 (2003) A244.
11. B. L. Ellis, K. T. Lee and L. F. Nazar, *Chem. Mater*., 22 (2010) 691.
12. O. K. Park, Y. H. Cho, S. H. Lee, H. C. Yoo, H. K. Song and J. Cho, *Energ. Environ. Sci.*, 4 (2011) 1621.
13. M. Hirayama, H. Ido, K. S. Kim, W. Cho, K. Tamura, J. Mizuki and R. Kanno, *J. Am. Chem. Soc*., 132 (2010) 15268.
14. A. Yamada, M. Tanaka, K. Tanaka and K. Sekai, *J. Power Sources*, 81 (1999) 73.
15. V. G. Kumar, J. S. Gnanaraj, S. B. David, D. M. Pickup, E. H. Eck and A. Gedanken, *Chem. Mater*., 15 (2003) 4211.
16. H. Y. Zhao, F. Li, X. Q. Liu, C. Chen, Z. Zhang, Y. Wu, W. Q. Xiong and B. Chen, *Electrochim. Acta*, 151 (2015) 263.
17. E. Hosono, T. Kudo, I, Honma, H. Matsuda and H. S. Zhou, *Nano lett*., 9 (2009)1045.
18. B. Li, X. G. Wei, Z. R. Chang, X. N. Chen, X. Z. Yuan and H. J. Wang, *Mater. Lett*., 135 (2014) 75.
19. Y. L. Ding, J. A. Xie, G. S. Cao, T. J. Zhu, H. M. Yu and X. B. Zhao, *Adv. Funct. Mater.*, 21 (2011) 348.
20. W. Tang, X. J. Wang, Y. Y. Hou, L. L. Li, H. Sun, Y. S. Zhu, Y. Bai, Y. P. Wu, K. Zhu and T. Ree, *J. Power Sources*, 198 (2012) 308.
21. D. K. Kim, P. Muralidharan, H. W. Lee, R. Ruffo, Y. Yang, C. K. Chan, H. L. Peng, R. A. Huggins and Y. Cui, *Nano lett*., 8 (2008) 3948.
22. Y. Yang, C. Xie, R. Ruffo, H. L. Peng, D. K. Kim and Y. Cui, *Nano lett*., 9 (2009) 4109.
23. D. Zhan, Q. G. Zhang, X. H. Hu, G. Z. Zhu and T. Y. Peng, *Solid State Ionics*, 239 (2013) 8.
24. Z. B. Wu, X. L. Pu, X. B. Ji, Y. R. Zhu, M. J. Jing, Q. Y. Chen and F. P. Jiao, *Electrochim. Acta*, 174 (2015) 238.
25. L. J. Xi, H. E. Wang, Z. G. Lu, S. L. Yang, R. G. Ma, J. Q. Deng and C. Y. Chung, *J. Power Sources*, 198 (2012) 251.
26. J. L. Li and F. Gao, *J. Power Sources*, 194 (2009) 1184.
27. W. Tang, Y. Hou, F. Wang, L. Liu, Y. Wu and K. Zhu, *Nano lett.*, 13 (2013) 2036.
28. W. Tang, S. Tian and L. Liu, *Electrochem. Commun.*, 13 (2011) 205.
29. X. Z. Sun, X. Zhang, H. T. Zhang, N. S. Xu, K. Wang and Y. W. Ma, *J. Power Sources*, 270 (2014) 318.
30. C. M. Bousquet, D. M. Rojas, W. J. Casteel, R. M. Pearlstein, G. G. Kumar, G. P. Pez and M. R. Palacín, *J. Power Sources*, 196 (2011) 1626.